


Impact of the Prediction Error on the Performance of Model Predictive Controllers with Long Prediction Horizons for Modular Multilevel Converters - Linear vs. Nonlinear System Models

Conference Paper

Author(s):

Fuchs, Simon; [Biela, Jürgen](#) 

Publication date:

2018

Permanent link:

<https://doi.org/10.3929/ethz-b-000328119>

Rights / license:

[In Copyright - Non-Commercial Use Permitted](#)

Impact of the Prediction Error on the Performance of Model Predictive Controllers with Long Prediction Horizons for Modular Multilevel Converters - Linear vs. Nonlinear System Models -

Simon Fuchs, Jürgen Biela
Laboratory for High Power Electronic Systems (HPE), ETH Zürich, Switzerland
Email: fuchs@hpe.ee.ethz.com

Keywords

«Modular Multilevel Converter», «Model Predictive Control», «Average Modelling»

Abstract

The closed loop control performance of MMCs can be significantly improved by using Model Predictive Control (MPC). This paper evaluates an MPC algorithm based on a linearised MMC model regarding the performance limits caused by the prediction error due to the linearisation. To decrease the prediction error to a minimum and to improve the performance it is proposed to use a nonlinear MMC model as a prediction model for the MPC. The steady state and transient performance of the MPC with both MMC models is compared in detail using simulations to analyse the effect of the prediction error on the control performance.

1 Introduction

Due to the multi-input multi-output (MIMO) characteristic of the Modular Multilevel Converter (MMC), the well known standard cascaded PI-controller structure (e.g. [1]) results in comparably low performance, when considering transients/reference steps or when dealing with relatively small inductance and module capacitance values. Also time delays due to sensing, communication and/or computation cannot be compensated properly with cascaded PI-controllers. Therefore, MIMO control schemes as for example in [2] were proposed. However, all these control schemes are not able to consider the system constraints like maximum output voltage of the individual MMC arms, maximum module voltage or arm/grid/DC currents. For example in case the output power of an MMC is reversed, the voltages of the module capacitors might increase above their maximum voltage if it is not considered in the control algorithm.

The control of MIMO systems with constraints is a typical application area of Model Predictive Control (MPC) algorithms. MPC algorithms perform an online prediction of the system's future behaviour and optimize the control input to find a tradeoff between tracking the (possibly contradicting) control references and the system constraints.

For MMCs, this could be beneficial, as one could decrease cost, volume and weight of the MMC by minimizing the inductance and capacitance values without losing (transient) performance, as the control takes the system's constraints into account. Therefore, the control performance benefits from long prediction horizons. For example, the module voltages might hit their maximum value constraints in the future after a reference step. If this is predicted by the control algorithm, a counteracting circulating current can be generated, such that the output currents are affected as little as possible by the constraint and an optimal trade off between meeting the constraints and tracking the reference can be implemented. There have been many predictive control schemes proposed for the MMC in the literature. Most of them consider the switching state of each module as the system input (e.g. [3, 4, 5, 6]). This results in a large integer optimization problem, such that in most cases only one prediction step is considered to not cause a too heavy computational burden. For large MMCs with high module numbers even a single prediction step can cause major computational problems.

In [7], not the switching state of the individual modules is considered, but the number of modules per arm, that are inserted. Consequently, instead of controlling the individual module voltages, the sum of all capacitor voltages of one arm is controlled. To keep the computational burden low, the change of the number of inserted modules per sampling instant is restricted to one module more or less. For a large number of modules, the restriction

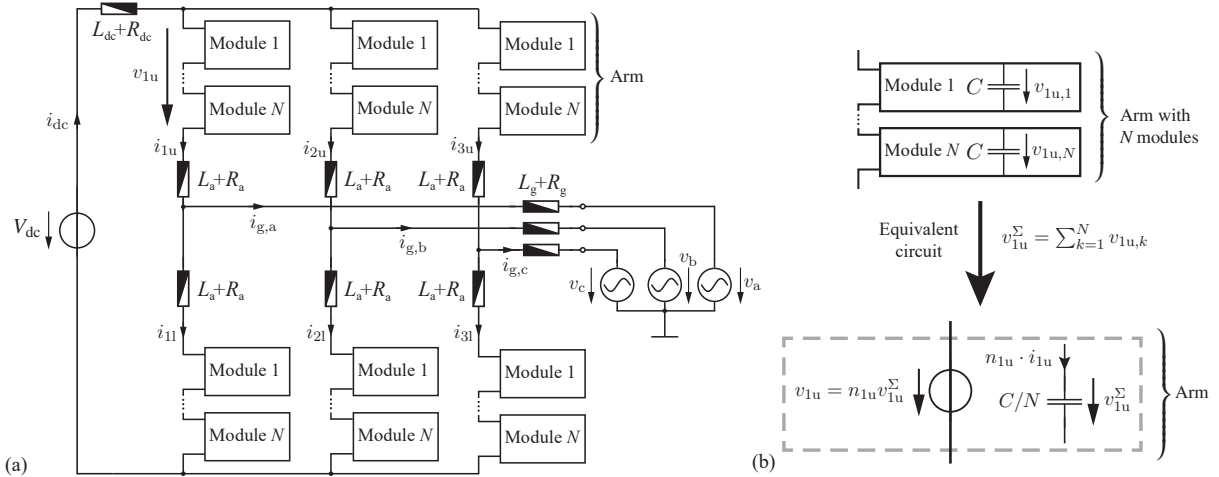


Fig. 1: (a) Three phase MMC. N modules form one out of six arms. (b) One arm can be represented as a (controllable) voltage source and a capacitor connected with a scaled current source. Here, the indices represent the upper arm of the first phase.

of inserting/bypassing not more one module per sampling instant results in slow reference tracking performance during transients.

Instead of controlling the individual modules' switching states with the MPC algorithm directly, a modulator can be used. The modulator typically uses a PWM to implement a given reference voltage for the individual arms. Modulators for MMCs can be designed such that all capacitor voltages within one arm are balanced around a mean value and the voltage reference is implemented at the output of the arm with only small errors [8, 9].

With a modulator, the MMC can be modelled by averaged models. This means that no actual switching states are considered. It is rather assumed that each MMC arm can generate a continuous output voltage. A common modelling approach is shown in Fig. 1(b), where the MMC arms are modelled with a capacitor fed by the arm current scaled with the so called insertion index n [10]. The insertion index can vary between zero and one and describes the share of inserted modules of the considered arm (1 for all modules inserted, 0 for all modules bypassed). The output voltage of the arm x is then the multiplication of the insertion index with the sum of all capacitor voltages v_x^Σ i.e. the internal arm voltage.

This average modelling with a modulator enables to use traditional MPC algorithms known from non switched systems. Therefore, the computational burden of the MPC algorithm is independent of the number of modules and can be used in many different application areas from medium voltage drive systems with few modules to HVDC converters with hundreds of modules [11]. In [12, 13] a bilinear MMC average model is linearised around the current operation point and a linear MPC algorithm based on a quadratic program (QP) is used to determine the reference voltages for the individual modulators of the MMC arms. The method allows long prediction horizons without a too heavy computational burden, as fast and efficient solvers for (linear) QPs are available. The problem of this method is the error of the prediction model that results from the linearisation. This error is dependant on the individual system parameters, especially the inductance values. If the error becomes too large, a long prediction horizon is worthless, because the prediction deviates too much from the real system's answer.

Based on the modelling method and the MPC algorithm from [12, 13] with changes to the cost function and reference formulation, this paper provides a short analysis of the resulting prediction error for different system parameters. To decrease the prediction error, it is proposed to utilize the nonlinear/bilinear MMC model directly as a prediction model in the MPC. Simulation results for validating both methods are shown. This demonstrates the benefit in control performance during transients as well as during steady state by having a correct prediction model.

The paper is organized as follows. After a short review of the mentioned MMC average modelling method presented in section 2 and the linearised MPC from [12, 13] with time varying references shown in section 3 and 4, the prediction error resulting from the linearisation is expressed analytically and discussed shortly for different inductance values in section 5. In section 6, a nonlinear MPC based on the nonlinear MMC model is presented as a benchmark for achieving low prediction errors. In section 7, simulation results are shown and analysed.

2 MMC Modelling

MPC algorithms require a model of the MMC in state space form. In this paper, the modelling proposed in [12], detailed in [13], is used. The following modelling section will always refer to the notation introduced in Fig.

1. Each arm has an insertion index n_{1u} that describes how much of the available inner arm voltage v_{1u}^Σ of the corresponding MMC arm is inserted into the arm, such that the reference voltage for an underlying modulator is equal to $n_{1u} \cdot v_{1u}^\Sigma$.

In the following, bold upper case letters denote a matrix, bold lower case letters a vector and regular lower case letters a scalar. According to [12], the MMC's dynamics in continuous time can be described with

$$\mathbf{i} = [i_{1u} \ i_{1l} \ i_{2u} \ i_{2l} \ i_{dc}]^T \quad \mathbf{v}^\Sigma = [v_{1u}^\Sigma \ v_{1l}^\Sigma \ v_{2u}^\Sigma \ v_{2l}^\Sigma \ v_{3u}^\Sigma \ v_{3l}^\Sigma]^T \quad \mathbf{v}_g = [v_{g,\alpha} \ v_{g,\beta}]^T$$

$$\frac{d}{dt} \begin{bmatrix} \mathbf{i} \\ \mathbf{v}^\Sigma \end{bmatrix} = \begin{bmatrix} \mathbf{L} & \mathbf{0} \\ \mathbf{0} & \mathbf{C}_a \end{bmatrix}^{-1} \cdot \left(\begin{bmatrix} -\mathbf{R} & \mathbf{K}_u \cdot \mathbf{N}(t) \\ \mathbf{N}(t) \cdot \mathbf{K}_i & \mathbf{0} \end{bmatrix} \cdot \begin{bmatrix} \mathbf{i} \\ \mathbf{v}^\Sigma \end{bmatrix} + \begin{bmatrix} \mathbf{K}_{vg} & \mathbf{K}_{dc} \\ \mathbf{0} & \mathbf{0} \end{bmatrix} \cdot \begin{bmatrix} \mathbf{v}_g \\ V_{dc} \end{bmatrix} \right), \quad (1)$$

with

$$\mathbf{L} = \begin{bmatrix} L_a & L_a & 0 & 0 & L_{dc} \\ 0 & 0 & L_a & L_a & L_{dc} \\ L_a & L_a & L_a & L_a & 2L_a + L_{dc} \\ L_g & -L_a - L & -L_g & L_a + L & 0 \\ 2L & -2L_a - 2L_g & L_g & -L_a - L_g & L_a \end{bmatrix}, \quad \mathbf{R} \text{ in the same manner}, \quad \mathbf{C}_a = \frac{C}{N} \cdot \mathbf{I}_{(6)}$$

$$\mathbf{K}_u = \begin{bmatrix} -1 & -1 & 0 & 0 & 0 & 0 \\ 0 & 0 & -1 & -1 & 0 & 0 \\ 0 & 0 & 0 & 0 & -1 & -1 \\ 0 & +1 & 0 & +1 & 0 & 0 \\ 0 & +1 & 0 & 0 & 0 & -1 \end{bmatrix}, \quad \mathbf{K}_i = \begin{bmatrix} 1 & 0 & 0 & 0 & 0 \\ 0 & 1 & 0 & 0 & 0 \\ 0 & 0 & 1 & 0 & 0 \\ 0 & 0 & 0 & 1 & 0 \\ -1 & 0 & -1 & 0 & 1 \\ 0 & -1 & 0 & -1 & 1 \end{bmatrix}$$

$$\mathbf{K}_{vg} = \begin{bmatrix} \mathbf{0}_{(3 \times 3)} \\ -1 & 1 & 0 \\ -1 & 0 & 1 \end{bmatrix}, \quad \mathbf{K}_{vdc} = [1 \ 1 \ 1 \ 0 \ 0]^T,$$

where $\mathbf{0}$ is a matrix of zeros and $\mathbf{I}_{(x)}$ is the identity matrix of dimension x . $\mathbf{N}(t)$ is the diagonal matrix of the vector containing the insertion indexes of all MMC arms $\mathbf{n}(t) = [n_{1u}(t) \ n_{1l}(t) \ n_{2u}(t) \ n_{2l}(t) \ n_{3u}(t) \ n_{3l}(t)]^T$. Note that (1) is a nonlinear/bilinear equation, because the system input $\mathbf{n}(t)$ is contained in the state coupling matrix.

3 Linearised MPC for MMCs (ℓ MPC)

To apply linear MPC to the MMC state space model (1), a linearization is proposed in [12, 13]. The linearisation is performed around an operation point using a first order Taylor series. The operation point is defined by the insertion indexes $\mathbf{n}(t_0)$, the currents $\mathbf{i}(t_0)$ and the inner arm voltages $\mathbf{v}^\Sigma(t_0)$. This results in the following system description:

$$\frac{d}{dt} \begin{bmatrix} \mathbf{i} \\ \mathbf{v}^\Sigma \end{bmatrix}_{\text{lin}} = \begin{bmatrix} \mathbf{L} & \mathbf{0} \\ \mathbf{0} & \mathbf{C}_a \end{bmatrix}^{-1} \cdot \left(\begin{bmatrix} -\mathbf{R} & \mathbf{K}_u \cdot \mathbf{N}(t_0) \\ \mathbf{N}(t_0) \cdot \mathbf{K}_i & \mathbf{0} \end{bmatrix} \cdot \begin{bmatrix} \mathbf{i} \\ \mathbf{v}^\Sigma \end{bmatrix}_{\text{lin}} + \begin{bmatrix} \mathbf{K}_u \cdot \mathbf{V}^\Sigma(t_0) \\ \mathbf{I}(t_0) \end{bmatrix} \cdot \Delta \mathbf{n}(t) + \begin{bmatrix} \mathbf{K}_{vg} & \mathbf{K}_{dc} \\ \mathbf{0} & \mathbf{0} \end{bmatrix} \cdot \begin{bmatrix} \mathbf{v}_g \\ V_{dc} \end{bmatrix} \right) \quad (2)$$

Here, $\mathbf{I}(t_0)$ is the diagonal matrix of $\mathbf{K}_i \cdot \mathbf{i}(t_0)$, $\mathbf{V}^\Sigma(t_0)$ is the diagonal matrix of $\mathbf{v}^\Sigma(t_0)$ and $\Delta \mathbf{n}(t) = \mathbf{n}(t) - \mathbf{n}(t_0)$. To be able to use the model (2) as a prediction model for a model predictive controller, a prediction of the grid voltage has to be added. By assuming the grid frequency ω to be constant for the prediction horizon,

$$\frac{d}{dt} \mathbf{v}_g = \begin{bmatrix} 0 & -\omega(t_0) \\ \omega(t_0) & 0 \end{bmatrix} \cdot \mathbf{v}_g = \mathbf{\Omega} \cdot \mathbf{v}_g \quad (3)$$

can be used to predict the grid voltage. Therefore, it has to be included into the state vector. The DC voltage V_{dc} is assumed to be constant during the whole prediction horizon.

Using the forward Euler approximation to discretise the resulting system with the sampling time T_s

$$\begin{bmatrix} \mathbf{i} \\ \mathbf{v}^\Sigma \\ \mathbf{v}_g \end{bmatrix}_{k+1} = \mathbf{x}_{k+1} = \left(\mathbf{I}_{(13)} + T_s \cdot \begin{bmatrix} \mathbf{L} & \mathbf{0} & \mathbf{0} \\ \mathbf{0} & \mathbf{C}_a & \mathbf{0} \\ \mathbf{0} & \mathbf{0} & \mathbf{I}_{(2)} \end{bmatrix}^{-1} \cdot \begin{bmatrix} \mathbf{0} & \mathbf{K}_u \mathbf{N}(t_0) & \mathbf{K}_{vg} \\ \mathbf{N}(t_0) \mathbf{K}_i & \mathbf{0} & \mathbf{0} \\ \mathbf{0} & \mathbf{0} & \mathbf{\Omega} \end{bmatrix} \right) \cdot \mathbf{x}_k + \quad (4)$$

$$T_s \cdot \begin{bmatrix} \mathbf{L} & \mathbf{0} & \mathbf{0} \\ \mathbf{0} & \mathbf{C}_a & \mathbf{0} \\ \mathbf{0} & \mathbf{0} & \mathbf{I}_{(2)} \end{bmatrix}^{-1} \cdot \left(\begin{bmatrix} \mathbf{K}_u \cdot \mathbf{V}^\Sigma(t_0) \\ \mathbf{I}(t_0) \\ \mathbf{0} \end{bmatrix} \cdot \Delta \mathbf{n}_k + \begin{bmatrix} \mathbf{K}_{dc} \\ \mathbf{0} \\ \mathbf{0} \end{bmatrix} \cdot V_{dc} \right) \quad (5)$$

$$= \mathbf{A}_{\text{lin},k} \cdot \mathbf{x}_k + \mathbf{B}_{\text{lin},k} \cdot \Delta \mathbf{n}_k \quad (6)$$

results as the prediction model. Note that due to the changing operation point during operation of the MMC, the system matrices have to be recalculated for every new sample. The outputs of the system are defined as the grid currents, the arm currents, the DC current and the inner arm voltages, such that

$$\mathbf{y}_k = [\mathbf{i}_{g,k} \quad \mathbf{v}_k^\Sigma \quad \mathbf{i}_{a,k} \quad i_{dc,k}]^T = \mathbf{C} \cdot \mathbf{x}_k \quad (7)$$

with $\mathbf{i}_{g,k} = [i_{g,a,k}, i_{g,b,k}, i_{g,c,k}]^T$ and $\mathbf{i}_{a,k} = [i_{u,1,k}, i_{l,1,k}, i_{u,2,k}, \dots, i_{l,3,k}]^T$.

The constraints for the MPC are:

- The insertion index that has to be between -1 and 1 for full-bridge modules or 0 and 1 for half-bridge modules.
- The absolute value of the arm currents must not exceed the rating of the semiconductors/inductors.
- The absolute value of the grid currents must not exceed the rating of the grid connection.
- The inner arm voltage must not exceed the maximum module voltage.

As presented in [13], all state constraints are implemented as soft constraints, such that the optimization problem results in

$$\mathbf{U}_{\ell\text{MPC},k} = \min_{\mathbf{U}} \sum_{l=k}^{k+N_p} \|\mathbf{Q} \cdot (\mathbf{y}_{l+1} - \mathbf{r}_{l+1})\|_2^2 + \|\mathbf{R} \cdot \mathbf{u}_l\|_2^2 + \lambda_{sc} \cdot \mathbf{1}_{(1 \times 16)} \cdot \boldsymbol{\xi}_{l+1} \quad (8a)$$

$$\text{s.t.: } \mathbf{x}_{l+1} = \mathbf{A}_{\text{lin},k} \cdot \mathbf{x}_l + \mathbf{B}_{\text{lin},k} \cdot \Delta \mathbf{n}_l \quad (8b)$$

$$\mathbf{y}_{l+1} = \mathbf{C} \cdot \mathbf{x}_{l+1} \quad (8c)$$

$$\mathbf{0}_{(16 \times 1)} \leq \boldsymbol{\xi}_{l+1} \quad (8d)$$

$$\mathbf{y}_{\max} - \mathbf{y}_{l+1} \leq \boldsymbol{\xi}_{l+1} \quad (8e)$$

$$-\mathbf{1}_{(6 \times 1)} - \mathbf{n}_{k-1} \leq \mathbf{u}_l \leq \mathbf{1}_{(6 \times 1)} - \mathbf{n}_{k-1} \quad \forall l = k \dots N_p - 1 \quad (8f)$$

$$\mathbf{U} = [\Delta \mathbf{n}_k \quad \Delta \mathbf{n}_{k+1} \quad \dots \quad \Delta \mathbf{n}_{k+N_p-1}]^T, \quad (8g)$$

where the cost weighting matrices \mathbf{Q} and \mathbf{R} are the diagonal matrices of the following vectors

$$\mathbf{q} = [\mathbf{1}_{(1 \times 3)} \lambda_{i_g} \quad \mathbf{1}_{(1 \times 6)} \lambda_{v_\Sigma} \quad \mathbf{1}_{(1 \times 6)} \lambda_{i_a} \quad \lambda_{i_{dc}}]^T \quad \text{and} \quad \mathbf{r} = \mathbf{1}_{(6 \times 1)} \lambda_u. \quad (9)$$

The ℓMPC is implemented in Matlab using the YALMIP toolbox [14] with the quadprog solver (Matlab integrated).

Reference values/trajectories are given for all outputs, as described in the next section.

4 Computation of the Reference Vector

The cost function shown in the previous section requires reference values r_{k+l} for all outputs y_{k+l} . The references are determined based on a DC current reference i_{dc}^* and a reference grid power angle $\phi = 0$ (PFC). The grid voltage $\mathbf{V}_{g,k}$ (in $\alpha\beta$ -coordinates), its amplitude $\hat{V}_{g,k}$ and the grid angle $\varphi_{g,k}$ are assumed to be known.

The grid currents' references are given by the power balance between AC and DC side, such that

$$\mathbf{i}_{g,l+1}^* = 2 \cdot \frac{V_{dc,k} \cdot i_{dc}^*}{3 \cdot \hat{V}_{g,k}} \cdot \begin{bmatrix} \sin(\varphi_{g,k} + \omega_g \cdot T_s \cdot (l+1-k)) \\ \sin(\varphi_{g,k} + \omega_g \cdot T_s \cdot (l+1-k) - 2\pi/3) \\ \sin(\varphi_{g,k} + \omega_g \cdot T_s \cdot (l+1-k) + 2\pi/3) \end{bmatrix}, \quad \forall l = k \dots N_p - 1. \quad (10)$$

Assuming that there are no circulating currents in steady state, the arm currents' references can be calculated from the DC and AC side currents with

$$\mathbf{i}_{a,l+1}^* = [+i_{g,a,l+1}^*/2 + i_{dc}^*/3, \quad -i_{g,a,l+1}^*/2 + i_{dc}^*/3, \quad \dots, \quad -i_{g,c,l+1}^*/2 + i_{dc}^*/3]^T, \quad (11)$$

$\forall l = k \dots N_p - 1$. The reference trajectories for the internal arm voltages can be computed via the power/energy equations of each arm (cf. e.g. [15]). Defining the grid voltage as $\hat{V}_g \cdot \sin(\omega_g t)$, the energy variation in the upper

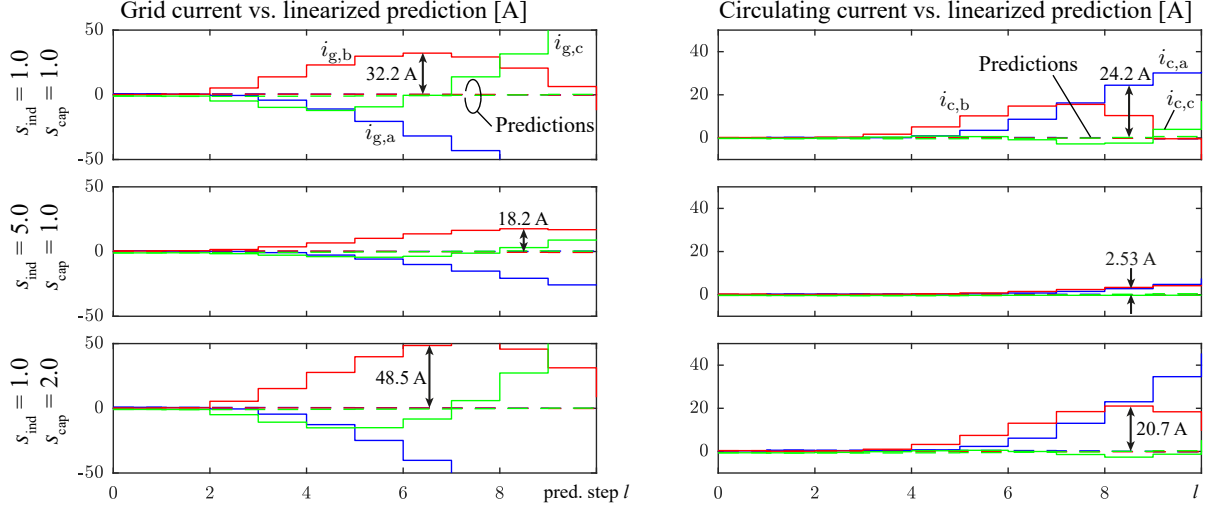


Fig. 2: Comparison between the nonlinear system's answer and the predicted answer of the linearised system for the grid and the circulating currents for different scalings of the system's passive components. The inductance values are scaled with s_{ind} , the capacitance values are scaled with s_{cap} as noted on the left hand side of the individual plots. Both references are zero. The data is taken from simulation results at $t = 3$ ms. The 0th prediction step represents the available measurement ($l = k$). The noted numerical values are exemplary chosen points to improve readability.

arm of phase 'a' is for example defined as

$$\Delta w_{1u,l+1}^* = \frac{S}{12m\omega_g} \cdot [4 \cdot \sin(\varphi_{g,k} + \omega_g T_s(l+1-k) - \phi - \pi/2) - m \cdot \sin(2\varphi_{g,k} + 2\omega_g T_s(l+1-k) - \phi - \pi)] - 2m^2 \cdot \sin(\varphi_{g,k} + \omega_g T_s(l+1-k) - \pi/2) \cdot \cos(\phi), \quad \forall l = k \dots N_p - 1, \quad (12)$$

with $m = 2 \cdot \hat{V}_{g,k} / V_{\text{dc},k}$ and $S = I_{\text{dc}}^* \cdot V_{\text{dc}}$. The internal arm voltage follows as

$$v_{1u,l+1}^{\Sigma*} = N \cdot \sqrt{2 \cdot (\Delta w_{1u,l+1}^* + \bar{w})} / C, \quad \forall l = k \dots N_p - 1. \quad (13)$$

The reference voltages for the other arms can be computed analogously.

5 Prediction Error

The linearisation shown in the previous section results in an (open loop) error for all predicted states. In the following, this error's sensitivity to the system parameters is investigated.

The prediction error can be calculated by subtracting (1) and (2):

$$\frac{d}{dt} \begin{bmatrix} \delta \mathbf{i} \\ \delta \mathbf{v}^{\Sigma} \end{bmatrix} = \begin{bmatrix} \mathbf{L} & \mathbf{0} \\ \mathbf{0} & \mathbf{C}_a \end{bmatrix}^{-1} \cdot \left(\begin{bmatrix} \mathbf{0} & \mathbf{K}_u \cdot \Delta \mathbf{N}(t) \\ \Delta \mathbf{N}(t) \cdot \mathbf{K}_i & \mathbf{0} \end{bmatrix} \cdot \begin{bmatrix} \delta \mathbf{i} \\ \delta \mathbf{v}^{\Sigma} \end{bmatrix} + \begin{bmatrix} \mathbf{K}_u \cdot \mathbf{V}^{\Sigma}(t_0) \\ \mathbf{I}(t_0) \end{bmatrix} \cdot \Delta \mathbf{n}(t) \right), \quad (14)$$

where $[\delta \mathbf{i}, \delta \mathbf{v}^{\Sigma}]^T$ denotes the difference $[\mathbf{i}, \mathbf{v}^{\Sigma}]^T - [\mathbf{i}, \mathbf{v}^{\Sigma}]_{\text{lin}}^T$ and $\Delta \mathbf{N}(t) = \mathbf{N}(t) - \mathbf{N}(t_0)$ denotes the diagonal matrix of the vector $\Delta \mathbf{n}(t)$. Note that the actual prediction error is different from (14) due to the Euler approximation used for the discretisation in the ℓ MPC.

The prediction error for an exemplary MMC system's grid and circulating currents (Table I and II) as well as its internal arm voltages is shown in Fig. 2 and 3 for different inductance and (module-) capacitance values. The inductance and capacitance values given in Table I where scaled by 5 or 2 respectively to point out the general trend for larger values. For large inductance values, the prediction errors of all quantities are smaller, whereas larger capacitance values do have a smaller impact on the error. Note, that for lower sampling frequencies, the error increases linearly.

As mentioned in the introduction, the advantage of a long prediction horizon is, that the controller can predict, if constraints will be hit in the future and react early enough to disturb the reference tracking of the outputs as little as possible. If the difference between the open loop prediction and the actual system response is too large, the controller predicts a wrong future behaviour of the system and thus can obtain only a suboptimal future input sequence.

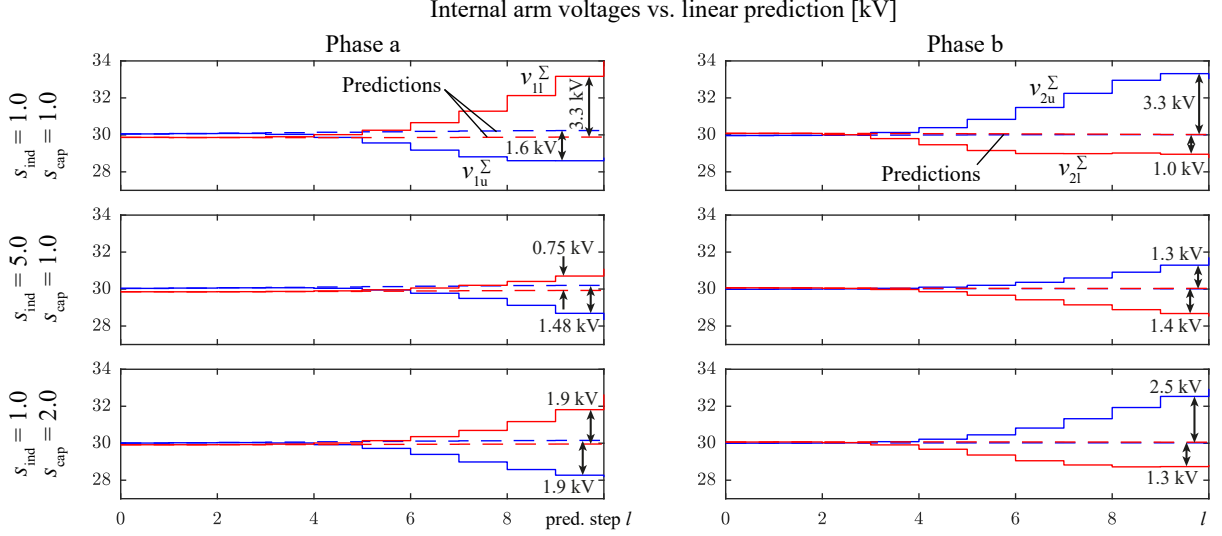


Fig. 3: Comparison between the nonlinear system's answer and the predicted answer of the linearised system for the inner arm voltages of phase a and b for different scalings of the system's passive components. The inductance values are scaled with s_{ind} , the capacitance values are scaled with s_{cap} as noted on the left hand side of the individual plots. The reference value is 30kV. The data is taken from simulation results at $t = 3$ ms. The 0th prediction step represents the available measurement ($l = k$). The noted numerical values are exemplary chosen points to improve readability.

6 Nonlinear MPC for MMCs (n MPC)

The nonlinear MPC presented in the following is based on the direct utilisation of the bilinear model (1) without the linearisation used in (2). The discretisation is done using the forward Euler approximation, such that

$$\mathbf{x}_{k+1} = \underbrace{\begin{bmatrix} \mathbf{L} & \mathbf{0} \\ \mathbf{0} & \mathbf{C}_a \end{bmatrix}^{-1} \cdot \left(\mathbf{I}_{(13)} + T_s \cdot \begin{bmatrix} -\mathbf{R} & \mathbf{K}_u \cdot \mathbf{N}_k \\ \mathbf{N}_k \cdot \mathbf{K}_i & \mathbf{0} \end{bmatrix} \right)}_{\mathbf{A}_{\text{nl}}(n_k)} \cdot \mathbf{x}_k + \underbrace{\begin{bmatrix} \mathbf{L} & \mathbf{0} \\ \mathbf{0} & \mathbf{C}_a \end{bmatrix}^{-1} T_s \cdot \begin{bmatrix} \mathbf{K}_{\text{dc}} & \mathbf{K}_{\text{vg}} \\ \mathbf{0} & \mathbf{0} \end{bmatrix}}_{\mathbf{B}_{V_{\text{dc,g}}}} \cdot \begin{bmatrix} V_{\text{dc},k} \\ V_{\text{g},k} \end{bmatrix} \quad (15)$$

is used as the prediction model. Note that the grid voltage prediction known from (3) is not included. This is done to avoid prediction errors in the grid voltage because of the discretisation with the Euler approximation. As there is no influence of the MMC on the grid voltage, one can predict the grid voltage separately using the exact (ZOH) discretisation of $\mathbf{\Omega}$ defined in (3).

The control law of the n MPC can be described as the following optimisation problem:

$$\mathbf{U}_{n\text{MPC},k} = \min_{\mathbf{U}} \sum_{l=k}^{k+N_p} \|\mathbf{Q}(\mathbf{y}_{l+1} - \mathbf{r}_{l+1})\|_2^2 + \|\mathbf{R}(\mathbf{n}_l - \mathbf{n}_{l-1})\|_2^2 + \lambda_{\text{sc}} \cdot \mathbf{1}_{(1 \times 16)} \cdot \boldsymbol{\xi}_{l+1} \quad (16a)$$

$$\text{s.t.: } \mathbf{x}_{l+1} = \mathbf{A}_{\text{nl}}(\mathbf{n}_l) \cdot \mathbf{x}_l + \mathbf{B}_{V_{\text{dc,g}}} \cdot [V_{\text{dc},k} \quad V_{\text{g},l}] \quad (16b)$$

$$\mathbf{N}_l = \text{diag}(\mathbf{n}_l) \quad (16c)$$

$$\mathbf{y}_{l+1} = \mathbf{C} \cdot \mathbf{x}_{l+1} \quad (16d)$$

$$-\mathbf{1}_{(6 \times 1)} \leq \mathbf{n}_l \leq +\mathbf{1}_{(6 \times 1)} \quad (16e)$$

$$\mathbf{0}_{(16 \times 1)} \leq \boldsymbol{\xi}_{l+1} \quad (16f)$$

$$\mathbf{y}_{\text{max}} - \mathbf{y}_{l+1} \leq \boldsymbol{\xi}_{l+1} \quad \forall l = k \dots N_p - 1 \quad (16g)$$

$$\mathbf{U} = [\mathbf{n}_k \quad \mathbf{n}_{k+1} \quad \dots \quad \mathbf{n}_{k+N_p-1}], \quad (16h)$$

where the definition of \mathbf{y} is the same as for the linearised prediction model presented in section 3. The definition of \mathbf{x} is also similar, as only the grid voltage is not part of \mathbf{x} anymore. The output references \mathbf{r} are defined as proposed in section 4.

To restrict undesired ripple in the DC current, the weighting matrices \mathbf{Q} and \mathbf{R} (see (9) for definition) are defined as time variant and an additional cost for the change of the DC current during the prediction period is introduced

Table I: MMC SYSTEM PARAMETERS

Symbol		SI value	pu value	Symbol		SI value	pu value
V_g	Grid voltage	9kV	$\sqrt{3}/2$	$I_{g,r}$	Rated grid current	22.681 A	1
S_r	Rated power	250kVA	1	$\omega_{g,r}$	Rated grid frequency	2π 50Hz	1
$V_{dc,r}$	Rated DC voltage	35kV	4.763	v_r^Σ	Rated inner arm voltage	30kV	4.083
L_g	Grid inductance	5mH	0.005	R_g	Grid resistance	0.5 Ω	0.0015
L_a	Arm inductance	26.8mH	0.026	R_a	Arm resistance	1 Ω	0.0031
L_{dc}	DC inductance	1.4 μ H	$1.4 \cdot 10^{-6}$	R_{dc}	DC resistance	20.6 m Ω	$63 \cdot 10^{-6}$
C	Module capacitance	159 μ F	16.216	N	Module number / arm	15	
$I_{g,max}$	max. grid current	30 A	1.323	$I_{a,max}$	max. arm current	50 A	2.2
$v_{C,max}$	max. module voltage	2.2kV	0.299	v_{max}^Σ	max. inner arm voltage	33kV	4.491

as follows.

$$\lambda_u = \begin{cases} 10 & \text{if reference step occurred less than 5 sampling periods ago,} \\ 20 & \text{else.} \end{cases} \quad (17)$$

The same is implemented for the DC current change cost $\lambda_{\Delta i_{dc}}$ that introduces a cost $J_{\delta i_{dc}}$ for the change in the DC current with

$$J_{\delta i_{dc}} = \sum_{l=k+1}^{k+N_p} \lambda_{\Delta i_{dc}} \cdot (i_{dc,l} - i_{dc,l-1}). \quad (18)$$

This additional cost can easily be integrated into \mathcal{Q} introducing the DC current change as an output with reference zero.

The optimisation problem resulting from (16)-(18) is implemented in Matlab using the YALMIP toolbox [14] with the `fmincon` solver (Matlab integrated).

Simulation results evaluating the performance of the n MPC are shown in the following section.

7 Simulation Results

In the following section, simulation results for the ℓ MPC and the n MPC applied on an exemplary MMC system are presented. The simulation is based on the average model of the MMC (cf. Fig. 1b)) and implemented in PLECS as well as Matlab Simulink, where a perfect modulation (no modulation error, cf. [8, 9]) is assumed. The system parameters are given in Table I. Note that the module capacities exceed the minimum value necessary for steady state operation at rated power [15] by 70%.

The simulation results are shown in Fig. 4. The simulation scenario is as follows: At the beginning, the current references are zero. At $t = 0.04$ s a reference step to the rated power occurs, before the power is reversed at $t = 0.129$ s. Note, that the second reference step is at the maximum value of the reference for the internal arm voltage of the upper arm of phase 'a' and therefore represents the worst case scenario in terms of the reference step size and the maximum voltage constraint, as the distance between the reference values before and after the reference step is the largest possible and the distance to the maximum value is the smallest possible.

The control performance with both the ℓ MPC and the n MPC is very good in steady state as well as during transients. The reference tracking of all outputs is fast and accurate. The performance differences between the linear and the nonlinear MPC formulations become clear when looking at the details:

- When the reference DC current/grid current is zero in the beginning of the simulation scenario, the ℓ MPC cannot keep the grid current lower than 2.612 A peak to peak, whereas the n MPC keeps it as low as 0.051 A (difference of -98 %).
- During steady state it is one of the control goals to meet the reference DC/grid current and inner arm voltages while keeping the occurring circulating currents as low as possible to save conduction losses. The n MPC (0.985 A peak to peak) can reduce the circulating currents by more than 50 % compared with the ℓ MPC (2.092 A peak to peak).
- Both, the ℓ MPC and the n MPC do not meet the DC reference current exactly during the time, when the

Table II: CONTROL SYSTEM PARAMETERS

Symbol	Meaning	SI value	pu value	Symbol	Meaning	SI value	pu value
T_s	Sampling time	1/1.5 kHz	0.2094	N_p	Prediction steps	10	
λ_{i_g}	Grid current cost		5	λ_{i_a}	Arm current cost		1
$\lambda_{i_{dc}}$	DC current cost		100	λ_{v_Σ}	Inner arm voltage cost		20
λ_u	Control output cost		20 or 10	$\lambda_{\Delta i_{dc}}$	DC current change cost		50 or 1
λ_{sc}	Soft constraints cost		10000				

reference is negative. Anyway, the ℓ MPC reaches a DC current error of 0.484 A, where the n MPC reaches 0.204 A. This is an improvement by 58 %.

- Looking at the second reference step at $t = 0.129$ s, one can notice that the n MPC achieves a faster rise time of the DC current. The same can be observed for the grid currents.
- Also the reference tracking of the inner arm voltages (thus the energy balancing) after the second reference step works better with the n MPC. To achieve this, the n MPC drives much larger circulating currents (the arm currents stay well within the limits of ± 50 A) directly after the reference step.

As the energy balancing/inner arm voltage reference tracking works very well and the constraints for the inner arm voltage are not fully exploited yet, the simulation scenario has been redone with module capacities that exceed the minimum value necessary for steady state operation at rated power [15] by only 10% resulting in a module capacitance value of 103.1 μ F (10.5 in pu). The results are shown in Fig. 5. All observations made for the results in Fig. 4 in tendency also apply for the reduces module capacitance simulation. Especially concerning the tracking of the DC current, the grid currents and the inner arm voltages, the n MPC outperforms the ℓ MPC. Only regarding the steady state circulating current amplitude, the difference between the two implementations is smaller than with the larger module capacitance.

8 Conclusion

After enhancing the linear MPC scheme (ℓ MPC) known from [12, 13] by adding time varying reference values for the internal arm voltages, the prediction error with linearized long prediction horizon MPC algorithms applied to MMCs is analysed. It is shown that the prediction error significantly depends on the individual system parameters such as the sampling frequency as well as the inductance and capacitance values. To identify the performance benefit of a more precise prediction model, using a nonlinear MMC model as a prediction model (n MPC) is proposed and the resulting control performance is compared to the linearisation based ℓ MPC using simulations.

Both of them perform very well. However, the n MPC's performance is concluded to be better during steady state (e.g. 50% less circulating currents and therefore lower losses) as well as during transients, where the DC/grid current reference is tracked faster and more accurate than with the ℓ MPC even if the constraints for the maximum inner arm voltage are active. A drawback of the n MPC algorithm are its high computational demand due to the non-linear optimisation problem that has to be solved in real time. This is only possible for relatively low sampling frequencies and/or with expensive computation hardware. The computation time to solve the nonlinear optimisation problem is up to 6 times longer than for the linear one (for Matlab implementation: maximum 2.4 s compared to 0.4 s). Therefore, this paper aimed to set a benchmark for the dynamic performance being achievable with MPC utilizing a good matching prediction model with low prediction errors.

In future works, the focus should be finding more precise prediction models without using nonlinear terms. However, with the currently ongoing progress in computing performance, solving nonlinear optimisation problems in real time might soon become a reasonable option even for power electronic systems. Another promising approach is explicit MPC, where the optimisation problem is solved offline and the solutions are stored in large look up tables, such that almost no computational power is required for the real time implementation and also high sampling frequencies are achievable.

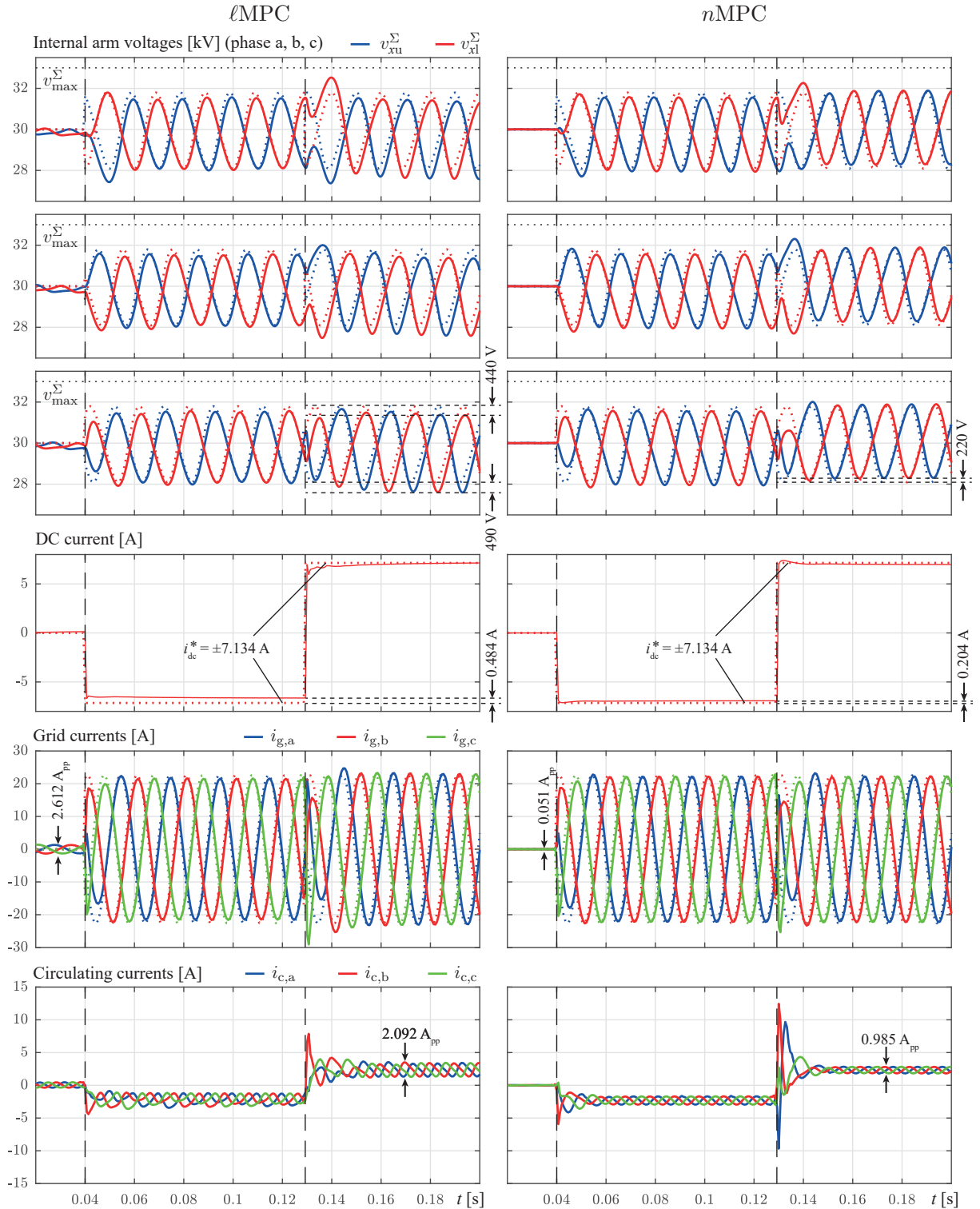


Fig. 4: Simulation results for the linearised ℓ MPC and the nonlinear n MPC applied on the MMC system described in Table I. References are shown as dotted lines, constraints (if existent) as horizontal dotted lines. The time instances, when the reference changes occur are marked with vertical dashed lines. For some examples, the steady state tracking errors are noted.

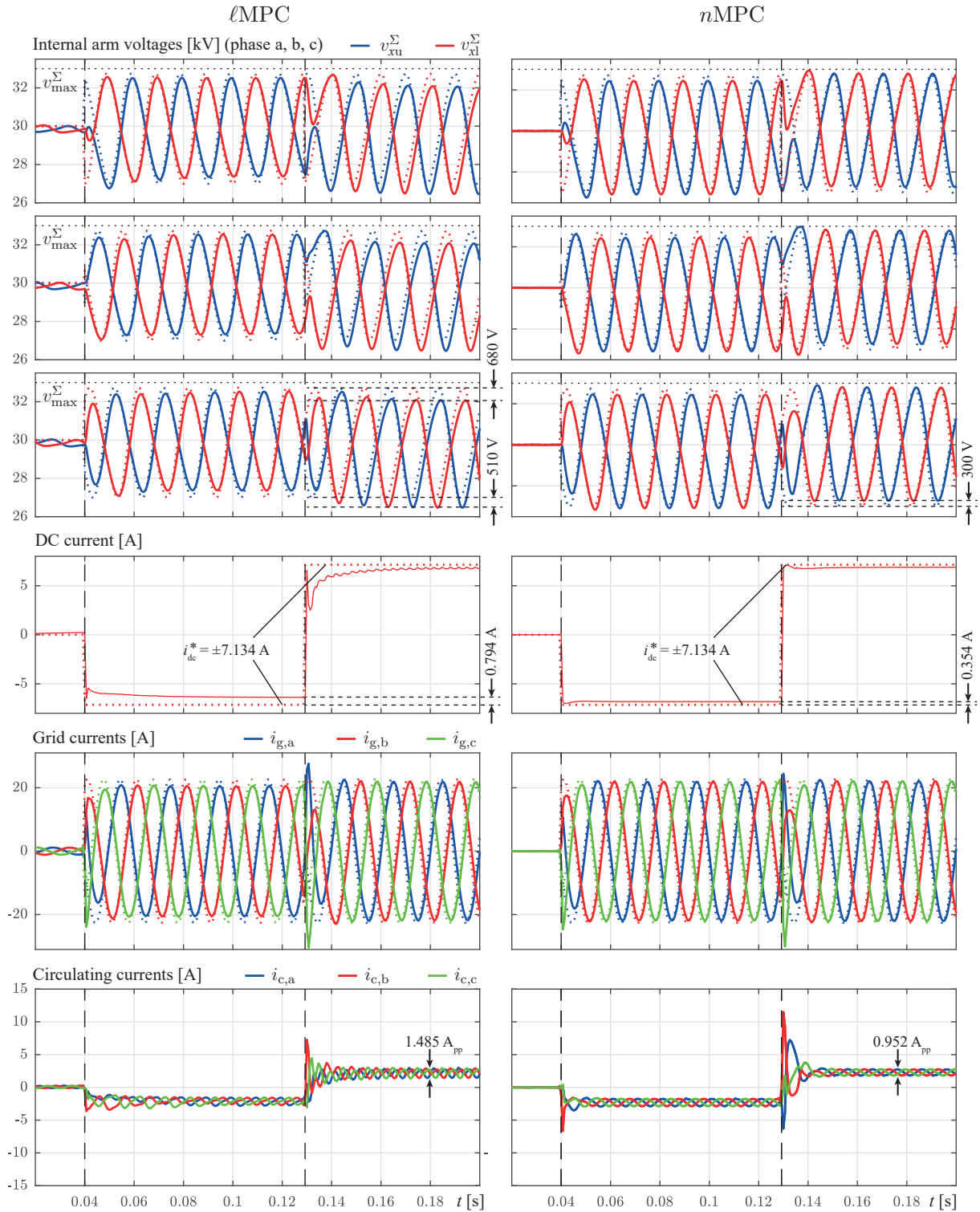


Fig. 5: Simulation results for the linearised ℓ MPC and the nonlinear n MPC applied on the MMC system described in Table I but with module capacitors of only $103.1\mu\text{F}$ (10.5 in pu). References are shown as dotted lines, constraints (if existent) as horizontal dotted lines. The time instances, when the reference changes occur are marked with vertical dashed lines. For some examples, the steady state tracking errors are noted.

Acknowledgements

This research is part of the activities of the Swiss Centre for Competence in Energy Research on the Future Swiss Electrical Infrastructure (SCCER-FURIES), which is financially supported by the Swiss Innovation Agency (Innosuisse - SCCER program).

References

- [1] J. Kolb, F. Kammerer, M. Gemminger, and M. Braun, "Cascaded control system of the modular multilevel converter for feeding variable-speed drives," *IEEE Trans. on Power Electronics*, vol. 30, no. 1, Jan 2015.
- [2] P. Münch, D. Görges, M. Izak, and S. Liu, "Integrated current control, energy control and energy balancing of modular multilevel converters," in *Conf. on IEEE Industrial Electronics Society (IECON)*, 2010.
- [3] J. Qin and M. Saeedifard, "Predictive control of a modular multilevel converter for a back-to-back HVDC system," *IEEE Trans. on Power Delivery*, vol. 27, 2012.
- [4] L. Ben-Brahim, A. Gastli, M. Trabelsi, K. A. Ghazi, M. Houchati, and H. Abu-Rub, "Modular multilevel converter circulating current reduction using model predictive control," *IEEE Transactions on Industrial Electronics*, vol. 63, no. 6, pp. 3857–3866, June 2016.
- [5] J.-W. Moon, J.-S. Gwon, J.-W. Park, D.-W. Kang, and J.-M. Kim, "Model predictive control with a reduced number of considered states in a modular multilevel converter for HVDC system," *IEEE Trans. on Power Delivery*, vol. 30, no. 2, Apr. 2015.
- [6] B. S. Riar, T. Geyer, and U. Madawala, "Model predictive direct current control of modular multilevel converters: Modeling, analysis, and experimental evaluation," *IEEE Trans. on Power Electronics*, vol. 30, no. 1, Jan. 2015.
- [7] M. Vatani, B. Bahrani, M. Saeedifard, and M. Hovd, "Indirect finite control set model predictive control of modular multilevel converters," *IEEE Trans. on Smart Grid*, May 2015.
- [8] S. Fuchs, S. Beck, and J. Biela, "High output voltage precision PWM for modular multilevel converters," in *19th Europ. Conf. on Power Electronics and Applications (EPE)*, Sept. 2017.
- [9] —, "Analysis and reduction of the output voltage error of PWM for modular multilevel converters," *IEEE Transactions on Industrial Electronics*, Jun 2018.
- [10] H. Bärnklaue, A. Gensior, and J. Rudolph, "A model-based control scheme for modular multilevel converters," *IEEE Trans. on Industrial Electronics*, vol. 60, no. 12, Dec 2013.
- [11] M. A. Perez, S. Bernet, J. Rodriguez, S. Kouro, and R. Lizana, "Circuit topologies, modeling, control schemes, and applications of modular multilevel converters," *IEEE Trans. on Power Electronics*, 2015.
- [12] G. Darivianakis, T. Geyer, and W. van der Merve, "Model predictive current control of modular multilevel converters," in *IEEE Energy Conversion Congress and Exposition (ECCE)*, 2014.
- [13] T. Geyer, *Model Predictive Control of High Power Converters and Industrial Drives*, L. John Wiley & Sons, Ed. John Wiley & Sons, Ltd., 2017, ISBN: 978-1-119-01088-3.
- [14] [Online]. Available: <https://yalmip.github.io/>
- [15] K. Ilves, S. Norrga, L. Harnefors, and H.-P. Nee, "On energy storage requirements in modular multilevel converters," *IEEE Trans. on Power Electronics*, vol. 29, no. 1, January 2014.